Enabling dynamic modelling of global coastal flooding by defining storm tide hydrographs

Job C. M. Dullaart[1], Sanne Muis[1,2], Hans de Moel[1], Philip J. Ward[1], Dirk Eilander[1,2], Jeroen C. J. H. Aerts[1,2]

1. Institute for Environmental Studies (IVM), Vrije Universiteit Amsterdam, Amsterdam, The Netherlands
2. Deltares, Delft, The Netherlands

Correspondence to: Job C. M. Dullaart (job.dullaart@vu.nl)

Abstract

Coastal flooding is driven by both high tides and/or storm surge, the latter being caused by strong winds and low pressure in tropical and extratropical. The combination of storm surge and the astronomical tide is defined as the storm tide. To gain understanding into the threat imposed by coastal flooding and to identify areas that are especially at risk, now and in the future, it is crucial to accurately model coastal inundation and assess the coastal flood hazard. Most models capable of simulating coastal inundation at the global scale follow a simple planar approach, often referred to as bathtub models. The main limitations of this type of model are that they implicitly assume an infinite flood duration and do not capture relevant physical processes. In this study we develop a method to generate hydrographs called HGRAPHER, and provide a global dataset of storm tide hydrographs. These hydrographs represent the typical shape of an extreme storm tide at a certain location along the global coastline. We test the sensitivity of the HGRAPHER method with respect to two main assumptions that determine the shape of the hydrograph, namely the surge event sampling threshold and coincidence in time of the surge and tide maxima. These hydrographs can be used to move away from planar to more advanced dynamic inundation modelling techniques at large scales.

1 Introduction

Over the course of the 21st century, coastal populations will be increasingly at risk of flooding due to sea level rise (SLR) (Oppenheimer et al., 2019). In addition, as a result of increasing exposure, the number of people living in coastal areas below 10 m elevation worldwide is projected to increase from over 600 million people today to more than 1 billion people by 2050 under all Shared Socioeconomic Pathways scenarios (Merkens et al., 2016). Global flood models can inform risk assessments that help to identify which areas are potentially exposed to flooding under both current and future climate conditions (Ward et al., 2015). Coastal flooding is generally driven by strong winds and low pressure in tropical (TCs) and extratropical cyclones (ETCs), which generate a storm surge (Resio and Westerink, 2008). The combination of storm surge and the tide is defined as the storm tide (Colle et al., 2010). Flood models can be used to model coastal inundation resulting from extreme storm tides.

Coastal inundation models have varying levels of complexity. Global models generally follow a simple planar approach (Brown et al., 2018; Dullaart et al., 2021a; Kirezci et al., 2020; Lincke and Hinkel, 2018; Muis et al., 2016). These models, often referred to as bathtub models, assume that any land that is below a specific static water level and that is connected to the sea will be inundated. The main limitation of the planar approach is that it assumes an infinite flood duration and does not capture the physical hydrodynamic processes (e.g. temporal evolution of a storm surge) that drive coastal

42   flooding. This can be partly addressed by accounting for water-level attenuation (Vafeidis et al., 2019;
43   Haer et al., 2018; Tiggeloven et al., 2020). Local to regional-scale models generally apply a
44   (hydro)dynamic modelling approach that captures the physical processes that drive flooding (Lewis et
45   al., 2013; Pasquier et al., 2019; Vousdoukas et al., 2018). Model comparisons at regional scale have
46   shown that in terms of flood extent and depth the dynamic modelling approach is more accurate than
47   the planar approach. Generally, the planar approach overestimates the flood extent due to the
48   assumption that flood propagation is only limited by topography, and that high water levels are
49   maintained for an infinite duration (Stephens et al., 2021). The main reasons for applying the planar
50   approach at the global scale, instead of the dynamic approach, are the simplicity of setting up a planar
51   model, low computational costs, and limited requirements for input data.

52   Due to the advances in high-performance computing and the development of reduced-physics
53   dynamic inundation models (Leijnse et al., 2021; Yin et al., 2016; Bates et al., 2010), there is the
54   potential to improve global flood mapping and step away from using the planar approaches for global
55   coastal inundation modelling. However, global flood maps are often derived for a specific return
56   period (RP), for example a flood map corresponding to the 1 in 100-year water level. While planar
57   models only need information about the height of the extreme water level, dynamic models also need
58   information about the duration. The temporal evolution of an extreme water level, composed of tide
59   and surge, is referred to as the hydrograph (Chbab, 2015; Sebastian et al., 2014; Salisbury and Hagen,
60   2007). Throughout this study we use the term hydrograph to refer to the storm tide hydrograph.
61   Hydrograph characteristics that determine the flood severity are, among others, the maximum storm
62   tide level, base duration, and overall shape. For example, when the water level is elevated for a longer
63   period of time the water will propagate further inland. Currently, a global dataset of hydrographs that
64   can be applied for dynamic inundation modelling for specific RPs is lacking. Vousdoukas et al. (2016)
65   made a first step towards dynamic inundation modelling at the continental-scale for Europe. In this
66   study, the temporal evolution of extreme water levels is incorporated by the use of a generic empirical
67   formulation. The surge hydrograph is assumed to be an isosceles triangle with a duration based on a
68   linear fit relationship between modelled surge heights and the half event duration. In reality the rising
69   and falling limb of the surge hydrograph can have a distinct shape that have different durations, and
70   varies from location to location (MacPherson et al., 2019). The tidal component is represented by
71   taking the highest tidal level from a 10-year period. Instead, a time-varying value could be used to
72   include tidal variation, including the spring-neap cycle, in a more accurate way. While some advances
73   have been made in modelling storm tide hydrographs, the current understanding of the temporal
74   evolution of sea levels during extremes is limited.

75   The aim of this study is to address this research gap by developing and applying a globally-applicable
76   method (HGRAPHER) to generate hydrographs. In doing so, we pave the way for global coastal flood
77   mapping using dynamic models. First, we review the various methods available to define a hydrograph
78   and their main assumptions. Second, building on the literature, we present the new open-source
79   HGRAPHER method with a global dataset of hydrographs for 23,226 locations along the world's
80   coastline. As input, we use storm surge and tide simulations (1979-2018) from the Global Tide and
81   Surge Model (GTSM) forced with the ERA5 climate reanalysis (Muis et al., 2020). Third, the sensitivity
82   of the HGRAPHER method is tested with respect to two main assumptions that determine the shape
83   of the hydrograph, namely: 1) using normal high tide or spring tide; and 2) the coincidence of the surge
84   and tide maximum or a time offset between the two maximums. Last, we discuss the limitations of
85   our methodology and ways forward.

2 Available methods to generate hydrographs

In this section we give an overview of four hydrograph generating methods. The reason for including these studies on hydrographs in this review, from the wide variety of studies that exists on this topic, is that they all have a clearly distinct methodology. Based on this review, we can select the hydrograph generating method that best fits our study goals. All four methods use multi-year water level time series from tide gauge stations or model simulations as input, but they differ in terms of input parameter used, the way the surge hydrograph is computed, and how tide and surge levels are combined. Table 1 summarizes the main characteristics of the four methods.

Table 1: Main characteristics of four hydrograph methods

study	study area	hydrograph method		
		input parameter	surge hydrograph	combine tide and surge
Chbab, 2015	Dutch coast	surge residual	averaging	linearly
Environment Agency, 2018	United Kingdom coast	skew surge	fit distribution	joint probability method
MacPherson et al., 2019	German Baltic Sea coast	storm tide	parametric	not required
Vousdoukas et al., 2016	European coast	surge and wave setup	best linear fit relationship	constant value for tide

The first method by Chbab (2015) starts by computing the residual water level. The surge residual is the difference between the predicted tide and the storm tide level (*Fig. 1*). Predicted tides are estimated by harmonic analyses to determine the amplitude and phase of the different tidal constituents. To define the surge hydrograph, events are selected from the residual time series by means of the Peaks-Over-Threshold (POT) method using 0.5 m as a threshold. The 36-hour period before and after the surge maximum is extracted. The final step to obtain the surge hydrograph is normalizing and averaging all 72-hour time series of surge levels. The surge hydrograph is added linearly to the average tidal cycle where the surge maximum is assumed to coincide with the tide maximum. To generate a hydrograph corresponding to a specific RP, the unitless surge hydrograph is scaled to a certain water level. For example, if the average maximum tide is 1 metre and the 100-year storm tide is 3 metres, the surge hydrograph is multiplied by 2. In areas with a large tidal range and a wide and shallow continental shelf, tide-surge interaction may induce a time offset between the two maxima (*Fig. 1*). For example, in the North Sea the surge maximum generally occurs 2.5 hours before the tidal maximum (Chbab, 2015; Horsburgh and Wilson, 2007). This is because a storm surge increases the depth and thereby modulates the influence of bottom friction and the speed of the tidal wave (Pugh, 1996; Rego and Li, 2010). The time offset can be taken into account by computing the time offset between the surge and tidal maxima for all surge events above the POT 99th percentile (POT99). Subsequently, the average offset is used to shift the surge time series relative to the tidal maximum.
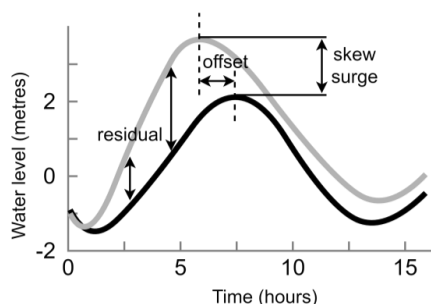
115

Figure 1: schematic of the residual, offset, and skew surge. Time series of the tide (grey line), and the tide including meteorological effects (black line) are shown.

116 The second method, developed by the U.K. Environment Agency (2018) starts by computing the skew
117 surge. Skew surge (*Fig. 1*) refers to the difference between the maximum storm tide level and
118 maximum tidal level within a tidal cycle, irrespective of their timing (Williams et al., 2016). An
119 important reason for using skew surge instead of the surge residual is that the latter can arise due to
120 tide-surge interaction (Idier et al., 2019). In contrast to the surge residual, for the skew surge there is
121 no need to account for timing offsets. To generate the skew surge hydrograph, the 15 most extreme
122 skew surges are selected. Both the high and low water skew surge values are extracted for each storm
123 event. Subsequently, the high and low water skew surge values are interpolated to a 15-minute
124 timeseries and normalized. Then, the duration of each of the 15 surges at particular percentiles (i.e.
125 10%, 20% and so on) are calculated. The maximum duration at each percentile is used to compute the
126 skew surge hydrograph. The study by U.K. Environment Agency does not combine the skew surge
127 hydrograph with tidal level time series.

128 The third method by MacPherson et al. (2019) starts by identifying storm tide events. To do this, a
129 POT method is used. Using POT is preferred over annual maxima because the number of events
130 extracted is typically higher with POT resulting in a more robust representation of the local storm tide
131 characteristics in the hydrograph. Then, each event is characterized through a parameterization
132 scheme. A total of 17 parameters are calculated such as peak water level, event duration, and the flow
133 (rising limb) and ebb (falling limb) curve shape. Subsequently, synthetic hydrographs are generated
134 through Monte Carlo simulations using the obtained parameters. This means that for a single return
135 period multiple storm tide hydrographs are available with different shapes but the same maximum
136 water level.

137 The fourth method by Vousdoukas et al. (2016) starts by computing the high tide water level (HTWL).
138 The HTWL is calculated as a constant water level that consists of the mean sea level (MSL) and the
139 maximum tide elevation taken from a 10-year time series. The HTWL is then combined with time-
140 varying storm surge levels and wave setup to obtain total water levels. Time series of storm surge
141 levels (1979-2014) are taken from Vousdoukas et al. (2016b) and wave setup is approximated by 20%
142 of the significant wave height, both based on the ERA-Interim global climate reanalysis (Dee et al.,
143 2011). To obtain information about the temporal evolution of an extreme event, extreme events are
144 identified in the available time series of surge and wave setup. For each identified event the duration
145 and peak water level are extracted. Subsequently, a best linear fit relationship between the duration
146 and peak water level is estimated. To conclude, the combined hydrograph consists of the HTWL
147 combined with a symmetric triangle shaped time series on top of it representing the surge and wave
148 setup for a certain return period.

149   Comparing the four methods, we find that the hydrograph generating methods that are developed for
150   application at smaller scales are tailored towards the local water level characteristics. This makes them
151   less suitable for application at larger scales. For example, in the study by Chbab (2015) a threshold of
152   0.5 m is used to identify extreme surge events in time series. However, at the global scale surge levels
153   exceeding 0.5 m do not occur in some regions such as the south of the Caribbean. The hydrograph
154   generating method developed by U.K. Environment Agency (2018) is developed for regions that
155   experience a substantial tidal range such as the U.K., as it is based on skew surge values. However, the
156   complete global coastline does not experience such high tides. In addition, MacPherson et al., (2019)
157   developed a method that is applicable in areas with a small tidal range, making it well suited for the
158   German Baltic Sea coast but inapplicable at larger scales. The last study that we discussed (Vousdoukas
159   et al., 2016a) takes a more simple approach to define hydrographs for continental Europe. The tidal
160   component is represented by a constant value and is combined with a triangle shaped time-varying
161   storm surge. Overall, the study by Vousdoukas et al. (2016a) is a step towards modelling inundation
162   at larger scales using hydrographs. However, substantial improvements can be made to the
163   hydrograph generating method. To this end, we will build on Chbab (2015) because, most importantly,
164   the method used in this study does take a time-varying surge and tide component into account. In
165   addition, instead of representing the surge by a triangle shape in the combined hydrograph like
166   Vousdoukas et al. (2016a), the method from Chbab (2015) allows the rising and falling limb of the
167   hydrograph to have different shapes. This results in a more accurate representation of the shape of
168   the storm surge in the combined hydrograph.

3 Methods

Figure 1 summarizes the main steps of the HGRAPHER hydrograph generating model. Storm tide levels, tidal time series, and storm tide RPs are used as input. First, extreme events are identified in the surge time series and used to compute a normalized surge hydrograph. Second, the average tide signal is computed from the tidal time series, Third, the hydrograph is generated by combining the average tide signal with the normalized surge hydrograph. To create the final hydrograph, this generic shape is scaled to an absolute water level height for specific RPs based on the COAST-RP dataset (Dullaart et al., 2021b).

3.1 Input data
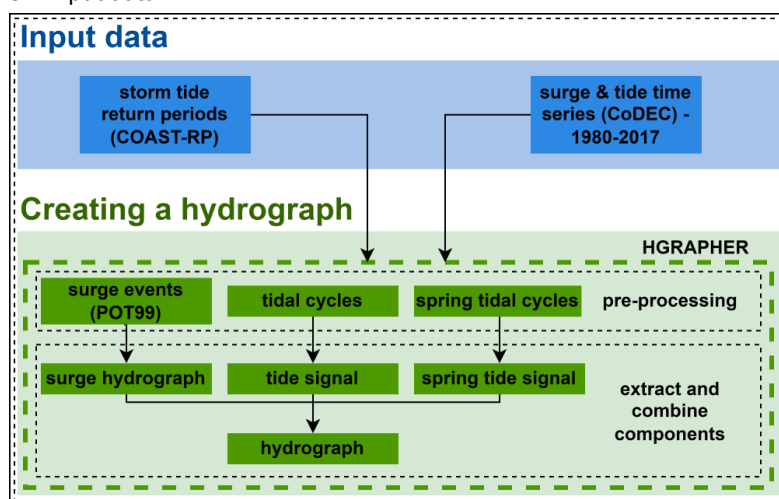
Figure 2: Modelling framework

Time series of storm tides (1980-2017) at a 10-minute interval from 23,226 output locations are taken from the CoDEC-ERA5 dataset (Muis et al., 2020). The CoDEC-ERA5 dataset was generated by forcing the 2D depth-averaged hydrodynamic Global Tide and Surge Model (GTSM) with wind and pressure fields from the ERA5 climate reanalysis (Hersbach et al., 2019). GTSM forced with ERA5 has shown to accurately simulate surge heights of historical TC and ETC events (Dullaart et al., 2020). In addition, a comparison between modelled and observed annual maxima, showed a mean bias of -0.04 m (with a standard deviation of 0.32 m) (Muis et al., 2020). Overall, the time series of surge and tidal levels from the CoDEC-ERA5 dataset are of good quality and therefore valid input data to HGRAPHER. The surge time series are computed as the difference between a storm tide simulation and a tide-only simulation. As a result, the surge time series include non-linear tide-surge interaction effects (Horsburgh and Wilson, 2007). The output locations are located at every 50 km along the coastline. In addition, the locations of tide gauge stations are included. In order to scale the hydrograph to a storm tide level that corresponds with a certain RP, we use storm tide RPs from the global COAST-RP dataset (Dullaart et al., 2021b). In contrast to other global storm tide RP datasets, COAST-RP explicitly takes into account low-probability high impact TCs (Dullaart et al., 2021a) by making use of 3,000 years of synthetic TC tracks from the STORM dataset (Bloemendaal et al., 2019).

194 ## 3.2 Creating a hydrograph

195 ### 3.2.1 Surge hydrograph
196 The following procedure is used for each of the 23,226 output locations individually. To generate a
197 hydrograph of the surge, we start with extracting independent extremes from the surge time series
198 based on the Peaks-Over-Threshold (POT) method. Using the POT method for selecting extremes is
199 preferred over annual maxima as the latter could result in excluding extreme events that happened in
200 the same year. We use the 99th percentile over the complete time series as threshold and we select
201 peaks that are at least 72 hours apart to ensure independent events (Wahl et al., 2017; Vousdoukas
202 et al., 2016b; Haigh et al., 2016). The threshold results in the selection of on average 1 surge event per
203 year and 40 events over the full time series. Setting the threshold is a trade-off between having an
204 event set of sufficient size to compute a representative average shape without including too many
205 relatively small surge events that would too strongly affect the resulting shape (see section 4.4). For
206 each selected surge event, we first extract the time series from 36 hours before, until 36 hours after
207 the peak (*Fig. 3a*). Second, each 72-hour surge event is normalized such that the maximum surge value
208 is equal to 1 (unitless). Third, we combine the selected surge events to calculate the average surge
209 hydrograph. This is done by determining the time (relative to the peak) at which a specific surge height
210 (from 0 to 1 with increments of 0.01) is exceeded. As an example, in Fig. 3a we show that for one surge
211 event the exceedance time at a normalized surge height of 0.25 is 14.0 hours before and 26.0 hours
212 (16.0 + 10.0) after the surge maximum occurred as indicated by the black arrows. Then, for each
213 normalized surge height the average exceedance time is computed, similar to Chbab (2015), resulting
214 in an average curve. Because the shape of the rising and falling limb of the surge can differ, the
215 exceedance time is calculated separately for each, and they are subsequently merged into the final
216 average surge hydrograph.
217
218 ### 3.2.2 Average and spring tide signal
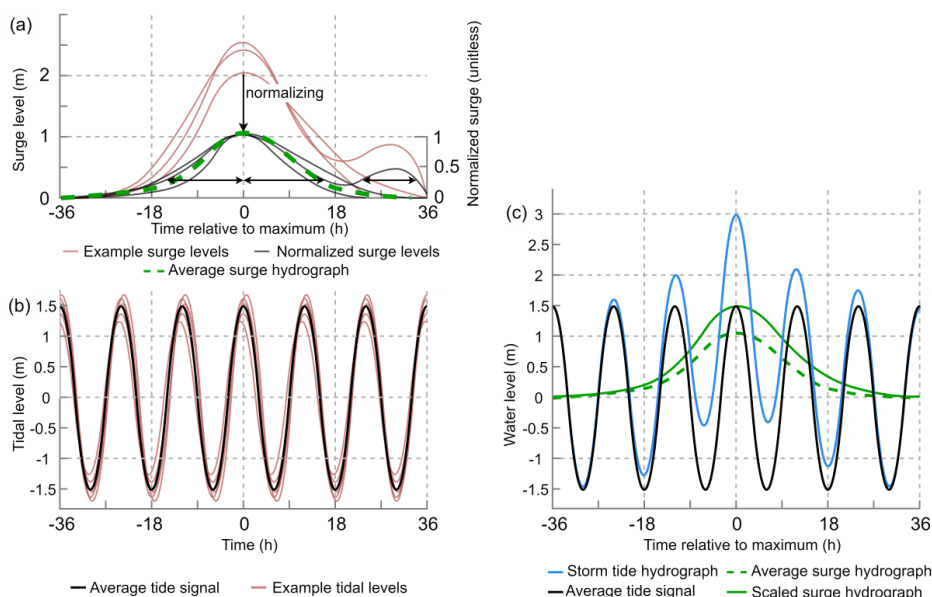
Figure 3: Visualization of the steps leading to the storm tide hydrograph of a hypothetical 1-in-100 year event of 3.0 m with the a) surge hydrograph, where the black arrows indicates the period over which a normalized surge height of 0.25 is exceeded. Note that for the falling limb we take the sum of the two time periods for which this is the case; b) average tide signal, and c) storm tide hydrograph. The average surge hydrograph is scaled to 1.5 m such that the combined water level equals the 1-in-100 year storm tide level of 3.0 m.

219   Next, we combine the surge hydrograph with the average tide signal (*Fig. 3b*). To create a curve
220   representing the average tide, we extract all tidal cycles of 24 hours and 50 minutes from the period
221   1980-2017. The start and end times of the tidal cycles are selected from the tide time series by
222   searching for a minimum around 24h and 50 minutes after the previous low tide. Last, we compute
223   the mean over all tidal cycles to extract the average tide signal.

224   In addition, we extract the spring tide signal because a storm surge event happening at spring tide can
225   result in a very different shape of the hydrograph. The spring-neap tide cycle takes two weeks. To
226   extract the average spring tide signal, we first search for the highest tide every two weeks. Second,
227   we select 72 hours of the tidal time series before and after the spring tide maximum. This procedure
228   is repeated for the available time series of the tide (1980-2017), after which we compute the mean
229   over all spring tides to extract the average spring tide signal.

230   3.2.3 Storm tide hydrograph
231   The surge hydrograph is combined with the average tide or spring tide to create a storm tide
232   hydrograph (*Fig. 3c*). In theory the surge maximum can coincide with any tide. However, in shallow
233   regions the timing will be influenced by interaction effects between the surge and the tide which
234   results in a phase difference. This is for example the case in the North Sea where the tidal wave will
235   start travelling faster under storm conditions due to the increased water level which reduces the
236   bottom friction (Horsburgh and Wilson, 2007; Resio and Westerink, 2008). To determine whether a
237   typical time offset between the surge and tide should be taken into account, we extract the
238   distribution of the timing offset between the surge and tidal maximum during the most extreme surge
239   events (POT99). For most locations around the globe, the distribution of the timing offset does not
240   show a clear signal (see section 4.4). Therefore, we assume that the surge and tidal maximum coincide.
241   With HGRAPHER a hydrograph can be generated for a total water level of interest. In this study we
242   use storm tide levels corresponding to a 100-year return period (RP100) because this is an often-used
243   coastal protection standard (Lamb et al., 2018; FEMA, 1968). If, for example, the RP100 storm tide
244   level is 3.0 meters and the average high tide is 1.5 meter this means the unitless average surge
245   hydrograph has to be scaled up to 1.5 meters, such that maximum surge plus the maximum tide is
246   equal to 3.0 meters (*Fig. 3c*).

4 Results

4.1 Storm surge hydrographs

For each output location from the CoDEC-ERA5 dataset, a surge hydrograph is generated. For illustration, results are shown for La Rochelle in France and Marco Island in the United States (*Fig. 4a & 4b*). We find a storm surge duration (i.e. the time over which the normalized surge height is above zero) of 54 hours in La Rochelle and 42 hours in Marco Island. Other studies find comparable storm surge durations of 40 hours for Hoek van Holland and 45 hours for Den Helder in The Netherlands (Chbab, 2015), and between 40 and 70 hours for the German Baltic Sea coast (MacPherson et al., 2019). The difference in storm surge duration between La Rochelle and Marco Island is likely caused by the different type of storm occurring in these regions. TCs can cause a fast shift from onshore to offshore winds when making landfall, which results in the surge becoming negative in just a couple of hours. Hurricane Irma is an example of a TC that made landfall near Marco Island and caused such a fast shift in surge levels. The normalized surge level time series have a strong irregular behaviour. This originates from the fact that the surge time series are obtained by subtracting tide-only simulations from a total water level simulations (including tidal and meteorological forcing). Therefore, the surge time series are the residual water level that include tide-surge interaction effects, and we believe this
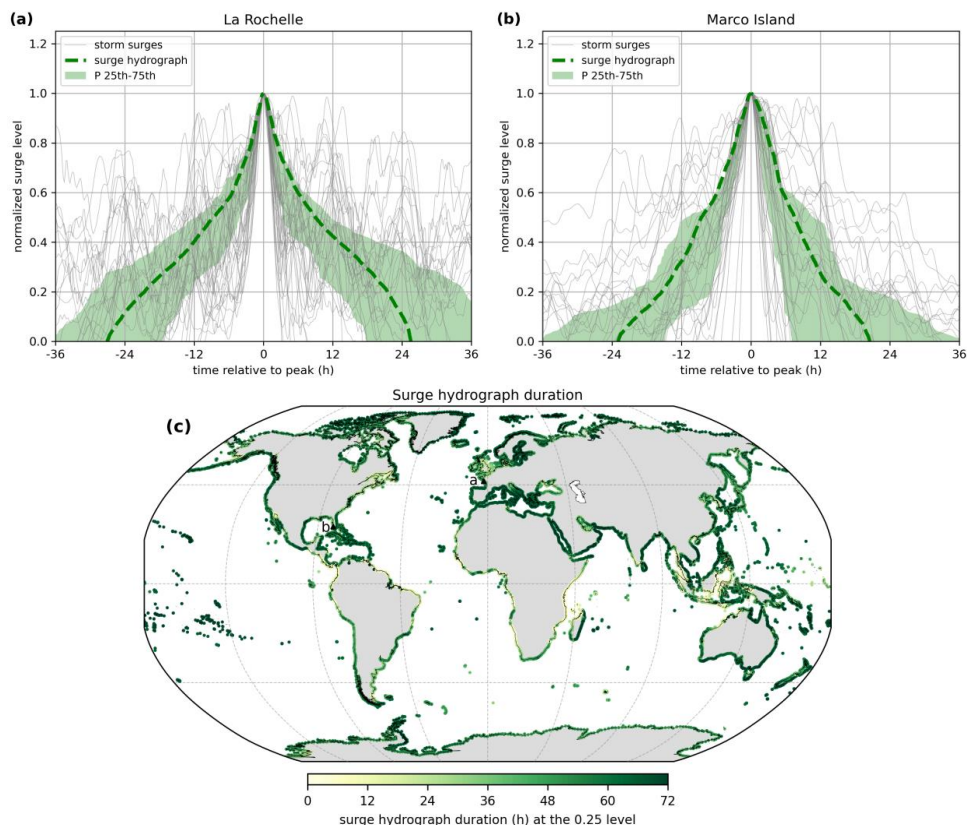
Figure 4: Surge hydrograph (dashed green line) for a) La Rochelle and b) Marco Island. Normalized surge levels are shown in grey and the green shaded area represents the $25^{th} - 75^{th}$ percentile. Panel c) shows the surge hydrograph duration at 0.25, with the locations of La Rochelle and Marco Island indicated by a and b, respectively.

263 partly explains the irregular behaviour. In addition, not all 40 events are extreme over their complete
264 lifetime, which means that noise is affecting the lower ends of the hydrograph. Taking the mean over
265 the normalized surge heights removes this irregular shape. At the global scale a distinct pattern shows
266 up in certain regions (*Fig. 4c*). In Europe for example, the average storm surge duration is substantially
267 lower in the North Sea compared to the Atlantic coastline and the Baltic Sea.

268 4.2 Average (spring) tide signal
269 For each output location the average and spring tide signal are computed. Although the tidal range at
270 La Rochelle is substantially larger than at Marco Island, the general shape of the average tide signal is
271 comparable (*Fig. 5a & 5b*). Both locations show a large variation in amplitude between tidal cycles.
272 For spring tide, the variation in the tidal amplitude between the tidal cycles is smaller. Note that the
273 grey shaded area exceeds the red shaded area at both locations during the first and third high tide
274 because the average spring tide signal is computed by taking the average over a two week period,
275 while the average tide signal is computed by taking the average over the daily tidal cycle of 24 hours
276 and 50 minutes. Furthermore, the duration of the first and second high and low tide cycle of a tidal
277 day differs at Marco Island. This is caused by the type of tide at this location which is a mixed
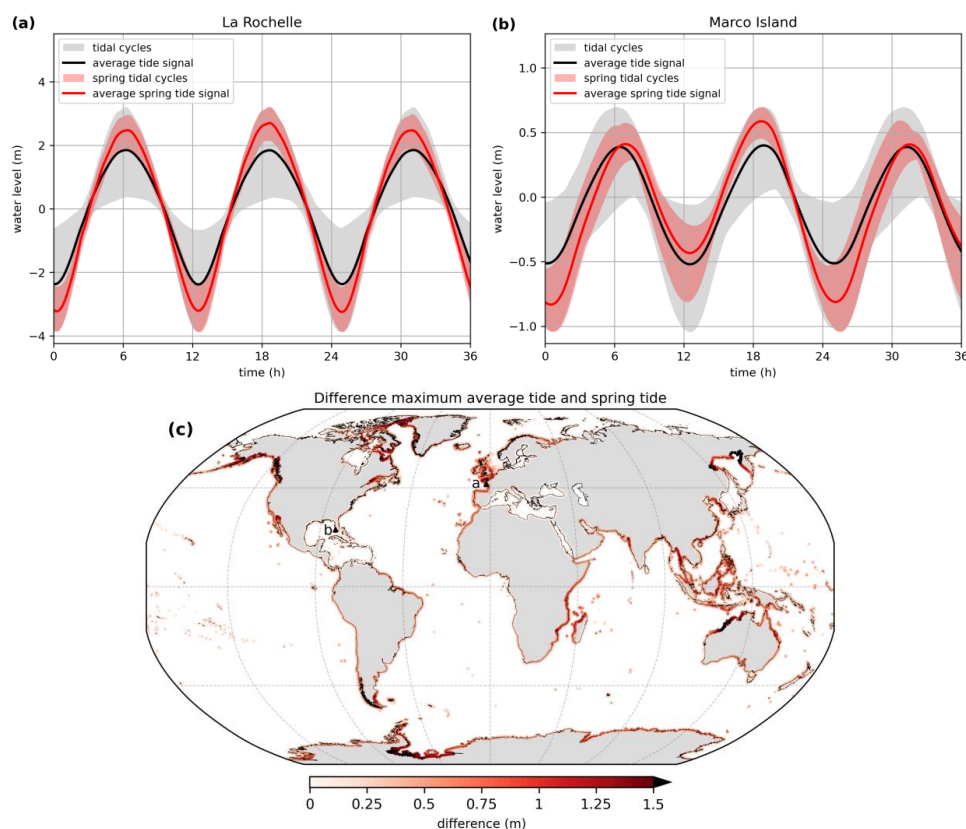
Figure 5: Average tide signal (black line) for a) La Rochelle and b) Marco Island. The grey shaded area shows the range of all tidal cycles. The average spring tide signal is shown in red and the red shaded area indicate all tidal cycles that are used to compute the average spring tide signal. Panel c) shows the absolute difference between the maximum average tide signal and average spring tide signal. The location of La Rochelle and Marco Island are indicated by the letters a and b, respectively.

278 semidiurnal tide (i.e. a tidal regime with two high and low tides per tidal day of different size) (Song
279 et al., 2011). Computing the average tide signal can be difficult at locations with a very small tidal
280 amplitude and mixed semidiurnal tide such a Montevideo (*Fig. A1*). Because of the large number of
281 shapes that the tidal cycles can have here, taking the average will not completely represent all possible
282 shapes. However, because the average high tide values are correctly represented by the average
283 (spring) tide signal, the findings are not affected to a large extent. For La Rochelle the maximum
284 average tide signal increases 46% from 1.85 m based on all tidal cycles to 2.70 m when taking the
285 average of the spring tidal cycles. In Marco Island the maximum average tide signal is 0.40 m and the
286 maximum average spring tide is 0.59 m (+48%). The larger absolute difference in La Rochelle means
287 that for an extreme storm tide to occur the timing of the surge maximum relative to the (spring) tide
288 maximum is more important compared to Marco Island. When applying HGRAPHER, it is important to
289 understand the typical characteristics of a storm tide in the area of interest, because this information
290 is needed to choose between the average and spring tide signal. For example, in northwest Australia
291 the difference between the maximum average and spring tide signal exceeds 1.5 m (*Fig. 5c*), indicating
292 that in this region an extreme storm tide is much more likely to occur during spring tide. Therefore,
293 using the average spring tide signal should be considered. At the global scale, the difference between
294 the average and spring tide signal maxima exceeds 0.5 m and 1.0 m, at 24% and 3% of all output
295 locations, respectively.

4.3 Storm tide hydrographs

The surge hydrograph is scaled up to a certain water level and combined with the average tide signal to obtain the storm tide hydrograph (*Fig. 6a and 6b*) that corresponds to the 1-in-100 year (RP100) storm tide level from the COAST-RP dataset (Dullaart et al., 2021b). In La Rochelle the RP100 storm tide level is 3.76 m and the average high tide is 1.85 m. Therefore, the unitless surge hydrograph is scaled up to 1.91 m, such that the combined water level equals the RP100 storm tide level. At Marco Island the RP100 storm tide level is 2.18 m to which the tide contributes 0.40 meter and the surge 1.78 meter, respectively. From the RP100 storm tide hydrograph that we create globally it is possible to deduce the relative contribution of the surge (*Fig. 6c*). Especially in areas where the maximum spring tide signal substantially exceeds (>0.5 m) the maximum average tide signal the surge contribution might be too large compared to observed historical events. This effect is counteracted by the assumption that the surge and tide coincide in time. As a result, a smaller surge is sufficient to get to the desired RP100 storm tide level compared to the situation where a time offset is implemented to combine the average tide signal with the scaled surge hydrograph.
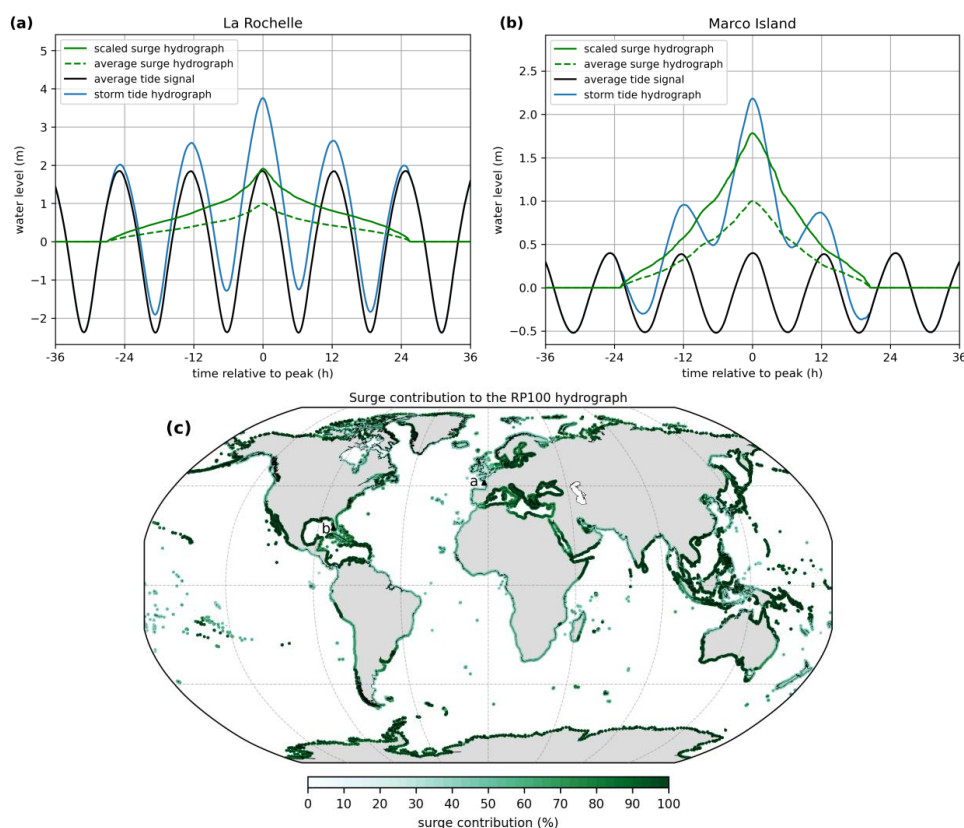
Figure 6: RP100 storm tide hydrograph (blue line) for a) La Rochelle and b) Marco Island. The average tide signal (black line), average surge hydrograph (green line), and scaled surge hydrograph (dashed green line) are also shown. Panel c) shows the relative contribution of the surge to the RP100 storm tide hydrograph maximum as a percentage. The locations of La Rochelle and Marco Island are indicated by the letters a and b, respectively.

4.4 Assumptions underlying the hydrograph

HGRAPHER is based on certain assumptions to create the storm tide hydrographs. Here, we aim to better understand how these assumptions influence the results. First, we assume that the POT99 threshold results in the selection of a set of surge events from the residual time series that represents the typical evolution of a surge event at any location. However, using a higher or lower POT percentile to select surge events will give different results, depending on the typical characteristics of a location. We illustrate this using La Rochelle and Marco Island as an example. Using a higher (POT99.5) or lower (POT98) POT percentile does not result in a clearly deviating surge hydrograph at La Rochelle (*Fig. 7*). At Marco Island however, a clear difference can be observe d between the surge hydrographs. Using the higher POT99.5 percentile (i.e. only using the ~20 most extreme surge events) results in a hydrograph that is more narrow and has a shorter duration. This is most likely caused by the different types of storms that occur at Marco Island. Using a higher POT percentile as threshold will result in an event set with a relatively larger share of TCs, compared to ETCs. This indicates that surge events caused by TCs are typically shorter compared to ETC-related surge events at Marco Island. Overall, to select the best POT percentile to generate the surge hydrograph, knowledge about the local conditions is required. For example, if surge events happen very infrequently (i.e. less than once per year) a percentile higher than POT99 should be used. Correspondingly, in areas where TCs occur such a higher POT percentile should be chosen if the research focusses on TCs. For this, knowledge about the number of historical TC storm surge events is required. Conversely, if the goal is to create a RP1 storm tide hydrograph a lower POT percentile is warranted compared to when one is interested in the RP100 storm tide hydrograph.
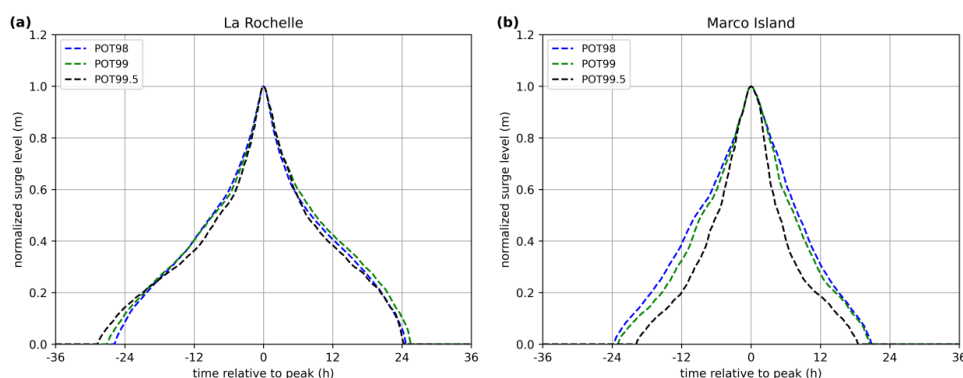
Figure 7: POT99 surge hydrograph (dashed green line) for a) La Rochelle and b) Marco Island. The blue and black dotted lines show the average surge hydrograph based on the surge events that exceed the POT98 and POT99.5 percentile.

Second, when combining the surge hydrograph with the average tide signal we assume that the maxima of the two coincide in time. Including a time offset will lead to a storm tide hydrograph of which the water level is elevated over a longer period of time, potentially increasing the severity of a flood event. To test this assumption we compute the time offset at La Rochelle and Marco Island (*Fig. 8a & 8b*), which is defined as the timing of the maximum storm tide relative to astronomical high tide (*Fig. 1*). What can be observed at both output locations is that the distribution is centred around zero. However, at Marco Island the distribution is more spread out, indicated by a standard deviation of 0.68 compared to 0.13 for La Rochelle. At the global scale, large mean absolute time offsets are observed in areas with either a very small tidal range, such as the Baltic Sea and the Mediterranean Sea, or a diurnal tide regime in combination with large TC induced storm surges, such as the Gulf of

341 Mexico (*Fig. 8c*). We show the absolute time offset instead of the actual values because this way all
342 areas where large time offsets occur are revealed, including areas with both positive and negative
343 time offsets. The globally averaged absolute mean offset is 33 minutes, and the median is 9 minutes.
344 To conclude, the assumption that the surge and tide maxima coincide is appropriate at most output
345 locations. However, at certain locations it should be considered to include a time offset when creating
346 a storm tide hydrograph.
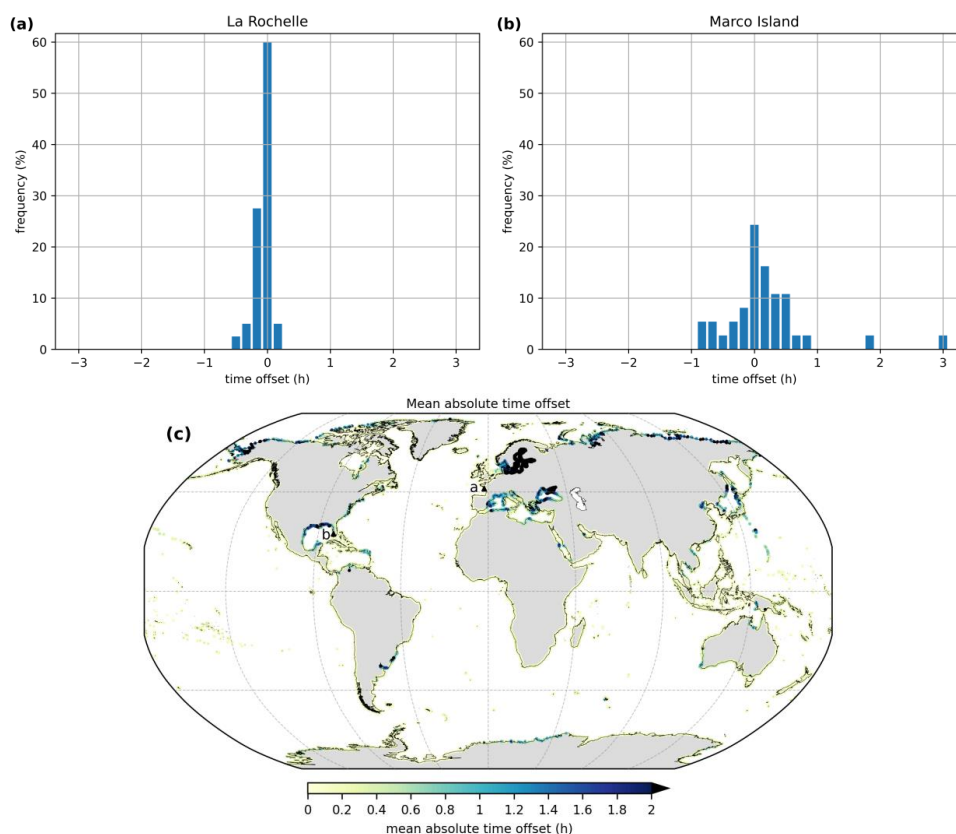
Figure 8: time offset distribution of the POT99 storm tide maxima relative to astronomical high tide at a) La Rochelle and b)
Marco Island. Each blue bar represents a 10-minute period. Panel c) shows the mean absolute time offset in hours. The
locations of La Rochelle and Marco Island are indicated by the letters a and b, respectively.

5 Discussion and conclusion

This study improves the global understanding of the duration and shape of extreme sea level events. It provides a novel global dataset of storm tide hydrographs which is a first step in moving away from the planar approach towards more dynamic inundation modelling at large scales. The open-source model that we developed that can generate hydrographs is called HGRAPHER and allows users to create storm tide hydrographs for a RP of interest. Here, we used time series of surge, tide and storm tide levels from the CoDEC dataset (Muis et al., 2020) and generated storm tide hydrographs with a 1-in-100 year return period based on COAST-RP (Dullaart et al., 2021b). Users have multiple options including, 1) use the average tide signal or spring tide signal; 2) define a POT percentile to select surge events for generating the surge hydrograph; 3) include a time offset for combining the surge hydrograph with the tide; 4) define for which RP a storm tide hydrograph should be generated; and 5) use other time series as forcing data for HGRAPHER.

Several aspects of our methodology could be further improved. First, surge level time series are obtained by subtracting tidal level time series from the storm tide level. As a result, the surge time series do not only contain the meteorological contribution to the sea level, but also contain tide-surge interaction effects, generally referred to as the residual water level (Horsburgh and Wilson, 2007). This could be addressed by using a 'surge-only' simulation, which would not be affected by interaction effects. Another aspect that could be improved is that our analysis is based on a 40 years timeseries. This provides a limited number of events, specifically for regions that do not regularly experience extremes such as the Caribbean. Potentially we could extend our analysis by using synthetic events, such as those presented for TCs in (Dullaart et al., 2021a). For extra-tropical regions, seasonal forecasts could be used to create a large ensemble of events. The advantage of a larger sample of events is that it would allow to assess if hydrographs are different for different RPs.

Second, we do not account for different types of storms. TCs and ETCs have distinct meteorological characteristics resulting in a different evolution of the water level over time. For example, TCs can have stronger wind speeds and lower air pressure than ETCs, resulting in a higher storm surge (Keller and DeVecchio, 2016). ETCs on the other hand generally affect a larger coastal area because they are often larger in size than TCs (Irish et al., 2008). In addition, once TCs move inland the wind direction can become offshore directly at the coast, resulting in a storm surge sign that quickly changes from positive to negative. An example of this is during TC Irma, which made landfall in Florida in 2017 (Cheng and Wang, 2019). A potential direction for future research would be to separate storm surges by type of storm that caused them and develop a surge hydrograph individually for TCs and ETCs.

Third, the average tide signal is computed by taking the average over thousands of tidal cycles with a duration of 1 lunar day, lasting 24 hours and 50 minutes. For the majority of the output locations HGRAPHER correctly extracts the average (spring) tide signal. However, in areas with a mixed tidal regime the daily uneven magnitude of the two high tides are averaged out. This is because over time it alters whether the first or second high tide is the highest tide during that lunar day. Including the mixed tidal regime characteristics at these locations, such as Montevideo (*App. A*), would result in a more realistic storm tide hydrograph. However, for this multiple storm tide hydrographs have to be generated that can be applied to different RPs. This makes the storm tide hydrographs dataset easy to implement in large scale flood hazard assessments.

A final limitation is that our analysis does not include waves. Wave setup can increase storm tide levels at the coast. Therefore, it is often an important component of extreme sea levels, and including a dynamic wave setup component in HGRAPHER is a potential direction for future research. To

391 accomplish this, we could make use of a parametric approach that has been used in previous global
392 scale studies to obtain estimates of wave setup (Vousdoukas et al., 2018; Kirezci et al., 2020).

393 HGRAPHER and the global dataset of storm tide hydrographs improve our understanding of the
394 duration and shape of storm tide levels. As a next step, the hydrographs could be applied in inundation
395 modelling and thereby provide a basis to move towards more dynamic inundation modelling at large
396 scales. More specifically, the storm tide hydrographs can be used as boundary conditions for large
397 scale dynamic inundation modelling. This way, the time component is taken into account when
398 modelling inundation which will substantially improve the accuracy of large-scale coastal flood hazard
399 assessments.

400 # 6 Appendices
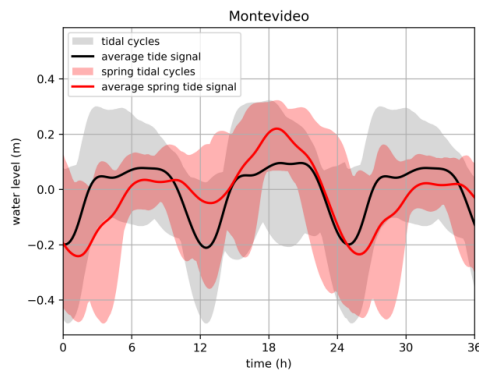
Figure A1: Average tide signal (black line) for Montevideo. The grey shaded area shows the range of all tidal cycles. The average spring tide signal is shown in red and the red shaded area indicate all tidal cycles that are used to compute the average spring tide signal.

401

7 Code availability

The HGRAPHER method developed in this study consists of several scripts that are available from GitHub at github.com/jobdullaart/HGRAPHER

8 Data availability

Sea level time series used in this study (CoDEC dataset) are available from the Copernicus Climate Data Store (CDS) at doi.org/10.24381/cds.8c59054f. In addition, the hydrographs generated in this study are available from the 4TU data repository at doi.org/10.4121/21270948.

9 Author contribution

JD developed the HGRAPHER method and wrote the paper. SM, HM, DE, PW, and JA participated in technical discussions and co-wrote the paper.

10 Competing interests

The authors declare that they have no conflict of interest.

11 Acknowledgements

We would like to thank Nathalie van Veen for her active involvement in the interpretation of the model outcomes and her critical look at the methodology. J.D. and J.A. received funding from the COASTRISK project financed by the SCOR Corporate Foundation for Science (R/003316.01). J.A. is also funded by the ERC Advanced Grant COASTMOVE #884442. S.M. received funding from the research program MOSAIC with project number ASDI.2018.036, which is financed by the Netherlands Organization for Scientific Research (NWO). D.E. and P.W. received funding from the NWO in the form of a VIDI grant (grant no. 016.161.324). This work was sponsored by NWO Exact and Natural Sciences for the use of supercomputer facilities (grant no. 2020.007).

12 References

Bates, P. D., Horritt, M. S., and Fewtrell, T. J.: A simple inertial formulation of the shallow water equations for efficient two-dimensional flood inundation modelling, J. Hydrol., 387, 33–45, https://doi.org/10.1016/j.jhydrol.2010.03.027, 2010.

Bloemendaal, N., Muis, S., Haarsma, R. J., Verlaan, M., Irazoqui Apecechea, M., de Moel, H., Ward, P. J., and Aerts, J. C. J. H.: Global modeling of tropical cyclone storm surges using high resolution forecasts, Clim. Dyn., 52, 5031, https://doi.org/10.1007/s00382-018-4430-x, 2019.

Brown, S., Nicholls, R. J., Goodwin, P., Haigh, I. D., Lincke, D., Vafeidis, A. T., and Hinkel, J.: Quantifying Land and People Exposed to Sea-Level Rise with No Mitigation and 1.5°C and 2.0°C Rise in Global Temperatures to Year 2300, Earth's Futur., 6, 583–600, https://doi.org/10.1002/2017EF000738, 2018.

Chbab, H.: Waterstandsverlopen kust. Wettelijk Toetsinstrumentarium WTI-2017, Delft, 2015.

Cheng, J. and Wang, P.: Unusual Beach Changes Induced by Hurricane Irma with a Negative Storm Surge and Poststorm Recovery, J. Coast. Res., 35, 1185–1199, https://doi.org/10.2112/JCOASTRES-D-19-00038.1, 2019.

Colle, B. A., Rojowsky, K., and Buonaito, F.: New York city storm surges: Climatology and an analysis of the wind and cyclone evolution, J. Appl. Meteorol. Climatol., 49, 85–100, https://doi.org/10.1175/2009JAMC2189.1, 2010.

Dee, D. P., Uppala, S. M., Simmons, A. J., Berrisford, P., Poli, P., Kobayashi, S., Andrae, U., Balmaseda, M. A., Balsamo, G., Bauer, P., Bechtold, P., Beljaars, A. C. M., van de Berg, L., Bidlot, J., Bormann, N., Delsol, C., Dragani, R., Fuentes, M., Geer, A. J., Haimberger, L., Healy, S. B., Hersbach, H., Hólm, E. V., Isaksen, L., Kållberg, P., Köhler, M., Matricardi, M., Mcnally, A. P., Monge-Sanz, B. M., Morcrette, J. J., Park, B. K., Peubey, C., de Rosnay, P., Tavolato, C., Thépaut, J. N., and Vitart, F.: The ERA-Interim reanalysis: Configuration and performance of the data assimilation system, Q. J. R. Meteorol. Soc., 137, 553–597, https://doi.org/10.1002/qj.828, 2011.

Dullaart, J. C. M., Muis, S., Bloemendaal, N., and Aerts, J. C. J. H.: Advancing global storm surge modelling using the new ERA5 climate reanalysis, Clim. Dyn., 54, 1007–1021, https://doi.org/10.1007/s00382-019-05044-0, 2020.

Dullaart, J. C. M., Muis, S., Bloemendaal, N., Chertova, M. V., Couasnon, A., and Aerts, J. C. J. H.: Accounting for tropical cyclones more than doubles the global population exposed to low-probability coastal flooding, Commun. Earth Environ., 2, 1–11, https://doi.org/10.1038/s43247-021-00204-9, 2021a.

Dullaart, J. C. M., Muis, S., Bloemendaal, N., Chertova, M., Couasnon, A., and Aerts, J. C. J. H.: COAST-RP: A global COastal dAtaset of Storm Tide Return Periods, https://doi.org/https://doi.org/10.4121/13392314, 2021b.

Environment Agency: Coastal flood boundary conditions for the UK: 2018 update, Bristol, 116 pp., 2018.

FEMA: The national flood insurance act of 1968, Natl. flood Insur. act 1968, 1968.

Haer, T., Botzen, W. J. W., Van Roomen, V., Connor, H., Zavala-Hidalgo, J., Eilander, D. M., and Ward, P. J.: Coastal and river flood risk analyses for guiding economically optimal flood adaptation policies: A country-scale study for Mexico, Philos. Trans. R. Soc. A Math. Phys. Eng. Sci., 376, https://doi.org/10.1098/rsta.2017.0329, 2018.

Haigh, I. D., Wadey, M. P., Wahl, T., Ozsoy, O., Nicholls, R. J., Brown, J. M., Horsburgh, K., and

470   Gouldby, B.: Spatial and temporal analysis of extreme sea level and storm surge events around the
471   coastline of the UK, Sci. Data, 3, 1–14, https://doi.org/10.1038/sdata.2016.107, 2016.

472   Hersbach, H., Bell, B., Berrisford, P., Horányi, A., Munoz Sabater, J., Nicolas, J., Radu, R., Schepers, D.,
473   Simmons, A., Soci, C., and Dee, D.: Global reanalysis: goodbye ERA-Inteirm, hello ERA5, ECMWF
474   Newsl., 159, 17–24, https://doi.org/10.21957/vf291hehd7, 2019.

475   Horsburgh, K. J. and Wilson, C.: Tide-surge interaction and its role in the distribution of surge
476   residuals in the North Sea, J. Geophys. Res. Ocean., 112, https://doi.org/10.1029/2006JC004033,
477   2007.

478   Idier, D., Bertin, X., Thompson, P., and Pickering, M. D.: Interactions Between Mean Sea Level, Tide,
479   Surge, Waves and Flooding: Mechanisms and Contributions to Sea Level Variations at the Coast,
480   Surv. Geophys., 40, 1603–1630, https://doi.org/10.1007/s10712-019-09549-5, 2019.

481   Irish, J. L., Resio, D. T., and Ratcliff, J. J.: The Influence of Storm Size on Hurricane Surge, J. Phys.
482   Oceanogr., 38, 2003–2013, https://doi.org/10.1175/2008JPO3727.1, 2008.

483   Keller, E. A. and DeVecchio, D. E.: Hurricanes and Extratropical Cyclones, in: Natural Hazards: Earth's
484   Processes as Hazards, Disasters, and Catastrophes, Routledge, New York, 331–363, 2016.

485   Kirezci, E., Young, I. R., Ranasinghe, R., Muis, S., Nicholls, R. J., Lincke, D., and Hinkel, J.: Projections of
486   global-scale extreme sea levels and resulting episodic coastal flooding over the 21st century, Sci.
487   Rep., 10, https://doi.org/10.1038/s41598-020-67736-6, 2020.

488   Lamb, R., Brisley, R., Hunter, N., Wingfield, S., Warren, S., Mattingley, P., and Sayers, P.: Flood
489   Standards of Protection and Risk Management Activities Final Report JBA Project Manager, North
490   Yorkshire, 74 pp., 2018.

491   Leijnse, T., van Ormondt, M., Nederhoff, K., and van Dongeren, A.: Modeling compound flooding in
492   coastal systems using a computationally efficient reduced-physics solver: Including fluvial, pluvial,
493   tidal, wind- and wave-driven processes, Coast. Eng., 163, 103796,
494   https://doi.org/10.1016/j.coastaleng.2020.103796, 2021.

495   Lewis, M., Bates, P., Horsburgh, K., Neal, J., and Schumann, G.: A storm surge inundation model of
496   the northern Bay of Bengal using publicly available data, Q. J. R. Meteorol. Soc., 139, 358–369,
497   https://doi.org/10.1002/qj.2040, 2013.

498   Lincke, D. and Hinkel, J.: Economically robust protection against 21st century sea-level rise, Glob.
499   Environ. Chang., 51, 67–73, https://doi.org/10.1016/j.gloenvcha.2018.05.003, 2018.

500   MacPherson, L. R., Arns, A., Dangendorf, S., Vafeidis, A. T., and Jensen, J.: A Stochastic Extreme Sea
501   Level Model for the German Baltic Sea Coast, J. Geophys. Res. Ocean., 124, 2054–2071,
502   https://doi.org/10.1029/2018JC014718, 2019.

503   Merkens, J. L., Reimann, L., Hinkel, J., and Vafeidis, A. T.: Gridded population projections for the
504   coastal zone under the Shared Socioeconomic Pathways, Glob. Planet. Change, 145, 57–66,
505   https://doi.org/10.1016/j.gloplacha.2016.08.009, 2016.

506   Muis, S., Verlaan, M., Winsemius, H. C., Aerts, J. C. J. H., and Ward, P. J.: A global reanalysis of storm
507   surges and extreme sea levels, Nat. Commun., 7, https://doi.org/10.1038/ncomms11969, 2016.

508   Muis, S., Apecechea, M. I., Dullaart, J., de Lima Rego, J., Madsen, K. S., Su, J., Yan, K., and Verlaan, M.:
509   A High-Resolution Global Dataset of Extreme Sea Levels, Tides, and Storm Surges, Including Future
510   Projections, Front. Mar. Sci., 7, https://doi.org/10.3389/fmars.2020.00263, 2020.

511   Oppenheimer, M., Glavovic, B. C., Hinkel, J., van de Wal, R., Magnan, A. K., Abd-Elgawad, A., Cai, R.,
512   Cifuentes-Jara, M., DeConto, R. M., Ghosh, T., Hay, J., Isla, F., Marzeion, B., Meyssignac, B., and

513 Sebesvari, Z.: Sea level rise and implications for low lying islands, coasts and communities, edited by:
514 Pörtner, H. O., Roberts, D. C., Masson-Delmotte, V., Zhai, P., Tignor, M., Poloczanska, E., Mintenbeck,
515 K., Alegría, A., Nicolai, M., Okem, A., Petzold, J., Rama, B., and Weyer, N. M., 2019.

516 Pasquier, U., He, Y., Hooton, S., Goulden, M., and Hiscock, K. M.: An integrated 1D–2D hydraulic
517 modelling approach to assess the sensitivity of a coastal region to compound flooding hazard under
518 climate change, Nat. Hazards, 98, 915–937, https://doi.org/10.1007/s11069-018-3462-1, 2019.

519 Pugh, D. T.: Tides, Surges and mean sea-level (Reprinted with corrections), John Wiley & Sons, Ltd.,
520 Chichester, U.K, 486 pp., https://doi.org/10.1016/0264-8172(88)90013-X, 1996.

521 Rego, J. L. and Li, C.: Nonlinear terms in storm surge predictions: Effect of tide and shelf geometry
522 with case study from Hurricane Rita, J. Geophys. Res. Ocean., 115, 1–19,
523 https://doi.org/10.1029/2009JC005285, 2010.

524 Resio, D. T. and Westerink, J. J.: Modeling the physics of storm surges, Phys. Today, 61, 33–38, 2008.

525 Salisbury, M. B. and Hagen, S. C.: The effect of tidal inlets on open coast storm surge hydrographs,
526 Coast. Eng., 54, 377–391, https://doi.org/10.1016/j.coastaleng.2006.10.002, 2007.

527 Sebastian, A., Proft, J., Dietrich, J. C., Du, W., Bedient, P. B., and Dawson, C. N.: Characterizing
528 hurricane storm surge behavior in Galveston Bay using the SWAN+ADCIRC model, Coast. Eng., 88,
529 171–181, https://doi.org/10.1016/j.coastaleng.2014.03.002, 2014.

530 Song, D., Wang, X. H., Kiss, A. E., and Bao, X.: The contribution to tidal asymmetry by different
531 combinations of tidal constituents, J. Geophys. Res. Ocean., 116, 1–12,
532 https://doi.org/10.1029/2011JC007270, 2011.

533 Stephens, S. A., Paulik, R., Reeve, G., Wadhwa, S., Popovich, B., Shand, T., and Haughey, R.: Future
534 changes in built environment risk to coastal flooding, permanent inundation and coastal erosion
535 hazards, J. Mar. Sci. Eng., 9, https://doi.org/10.3390/jmse9091011, 2021.

536 Tiggeloven, T., De Moel, H., Winsemius, H. C., Eilander, D., Erkens, G., Gebremedhin, E., Diaz Loaiza,
537 A., Kuzma, S., Luo, T., Iceland, C., Bouwman, A., Van Huijstee, J., Ligtvoet, W., and Ward, P. J.: Global-
538 scale benefit-cost analysis of coastal flood adaptation to different flood risk drivers using structural
539 measures, Nat. Hazards Earth Syst. Sci., 20, 1025–1044, https://doi.org/10.5194/nhess-20-1025-
540 2020, 2020.

541 Vafeidis, A. T., Schuerch, M., Wolff, C., Spencer, T., Merkens, J. L., Hinkel, J., Lincke, D., Brown, S., and
542 Nicholls, R. J.: Water-level attenuation in broad-scale assessments of exposure to coastal flooding: a
543 sensitivity analysis, Nat. Hazards Earth Syst. Sci., 19, 973–984, https://doi.org/10.5194/nhess-2018-
544 359, 2019.

545 Vousdoukas, M. I., Voukouvalas, E., Mentaschi, L., Dottori, F., Giardino, A., Bouziotas, D., Bianchi, A.,
546 Salamon, P., and Feyen, L.: Developments in large-scale coastal flood hazard mapping, Nat. Hazards
547 Earth Syst. Sci., 16, 1841–1853, https://doi.org/10.5194/nhess-16-1841-2016, 2016a.

548 Vousdoukas, M. I., Voukouvalas, E., Annunziato, A., Giardino, A., and Feyen, L.: Projections of
549 extreme storm surge levels along Europe, Clim. Dyn., 47, 1–20, https://doi.org/10.1007/s00382-016-
550 3019-5, 2016b.

551 Vousdoukas, M. I., Mentaschi, L., Voukouvalas, E., Verlaan, M., Jevrejeva, S., Jackson, L. P., and
552 Feyen, L.: Global probabilistic projections of extreme sea levels show intensification of coastal flood
553 hazard, Nat. Commun., 9, 2360, https://doi.org/10.1038/s41467-018-04692-w, 2018.

554 Wahl, T., Haigh, I. D., Nicholls, R. J., Arns, A., Dangendorf, S., Hinkel, J., and Slangen, A. B. A.:
555 Understanding extreme sea levels for broad-scale coastal impact and adaptation analysis, Nat.

556   Commun., 8, 1–12, https://doi.org/10.1038/ncomms16075, 2017.

557   Ward, P. J., Jongman, B., Salamon, P., Simpson, A., Bates, P., De Groeve, T., Muis, S., De Perez, E. C.,
558   Rudari, R., Trigg, M. A., and Winsemius, H. C.: Usefulness and limitations of global flood risk models,
559   Nat. Clim. Chang., 5, 712–715, https://doi.org/10.1038/nclimate2742, 2015.

560   Williams, J., Horsburgh, K. J., Williams, J. A., and Proctor, R. N. F.: Tide and skew surge independence:
561   New insights for flood risk, Geophys. Res. Lett., 43, 6410–6417,
562   https://doi.org/10.1002/2016GL069522, 2016.

563   Yin, J., Lin, N., and Yu, D.: Coupled modeling of storm surge and coastal inundation: A case study in
564   New York City during Hurricane Sandy, Water Resour. Res., 52, 8685–8699,
565   https://doi.org/10.1002/2016WR019102, 2016.

566